Solid-State Electronics Vol. 30, No. 4, pp. 445–455, 1987
Printed in Great Britain.

0038-1101/87 $3.00 + 0.00

TWO-DIMENSIONAL MODELING OF ION IMPLANTATION WITH SPATIAL MOMENTS

G. HOBLER, E. LANGER and S. SELBERHERR
Institut fuer Allgemeine Elektrotechnik und Elektronik, Technische Universitaet Wien, Gusshausstrasse 27-29, A-1040 Wien, Austria

(*Received* 12 *May* 1986; *in revised form* 17 *September* 1986)

Abstract—We present a two-dimensional model of ion implantation which allows for position dependent lateral moments. The lateral standard deviation and the lateral kurtosis as a function of depth have been calculated by 2-D Monte-Carlo simulations for boron, phosphorus, arsenic, and antimony in silicon for energies in the range of 10–300 keV. The lateral moments as a function of depth and energy as well as the vertical moments as a function of energy have been fitted by simple formulae. We specify two types of distribution functions the parameters of which can be adjusted to given values of standard deviation and kurtosis. In this way the depth dependent lateral moments can be included into analytical distribution functions.

1. INTRODUCTION

For the purpose of describing ion implantation profiles, methods based on distribution functions together with spatial moments have now been used for more than 20 years. The principle of these methods is to assume a functional type for the distribution function and to calculate its free parameters from its spatial moments. These moments may be obtained either by experiment or by theory. For a long time only the first two moments, i.e. the mean projected range and the projected range straggling (the standard deviation), could be specified[1] and so the only reasonable distribution function was the Gaussian function. A first step of sophistication was carried out by Gibbons in 1973[2], who proposed to use joined half-Gaussian distributions to take into account moderate profile asymmetry. Although these oldest models are still frequently used for the sake of simplicity or for lack of higher moments[3–4], it is well established today that for a realistic description of 1-D profiles 4 moments must be taken into account. For this purpose the Pearson IV distribution is commonly used[5–9] which was introduced by Hofker in 1975[10].

The first model including lateral spread was presented by Furukawa in 1972[11]. It is based on the statistical distribution function for one ion, i.e. the response to a punctiform beam. By a convolution of this distribution function he obtained the distribution under an infinitely steep and infinitely high mask edge. Later this model was extended to the case of arbitrarily shaped mask edges by Runge[12] and further models were developed to allow for different stopping powers of mask and bulk material[13–16,9].

In this paper we will give a sophisticated model for the statistical distribution function of one ion. We denote it $f(z, x)$, with z the vertical coordinate (perpendicular to the surface) and x the lateral coordinate. $z = x = 0$ is the point of entrance of the ion. Furukawa and still Runge used a 2-D Gaussian function for $f(z, x)$, which may be written:

$$f(z, x) = \text{gauss}(z)\,\text{gauss}(x). \tag{1}$$

This approach has been refined by Ryssel [17] to:

$$f(z, x) = f_{\text{vert}}(z)\,\text{gauss}(x), \tag{2}$$

with $f_{\text{vert}}(z)$ a proper 1-D distribution function. Using a Pearson *IV* function, today's standard model reads:

$$f(z, x) = \text{pears}\,(z)\,\text{gauss}(x). \tag{3}$$

The major limitation of this description is that it ignores any correlation between the vertical (z) and the lateral (x) coordinate, or to say it in other words, that the lateral standard deviation is assumed to be independent of the depth. Furthermore, assuming a Gaussian distribution, no higher lateral moments are taken into account. Our Monte-Carlo simulations indicate that these assumptions are not correct. In Figures 1 and 2 the lateral standard deviation and the lateral kurtosis are shown, respectively, as a function of depth for the case of a 100 keV implantation of arsenic into silicon (dashed lines). As a reference the vertical distribution function (histogram) is also depicted.

The impact on the distribution by a vertical mask edge is shown in Figs 3 and 4. The standard model (Fig. 3) is compared with the results of our Monte-Carlo simulation (Fig. 4) of a 200 keV boron implantation into silicon. This example has been chosen because boron has a very large lateral standard deviation. One can see that the classical distribution extends too far below the mask at the maximum concentration of the vertical profile and not far enough at regions closer to the surface. The reason

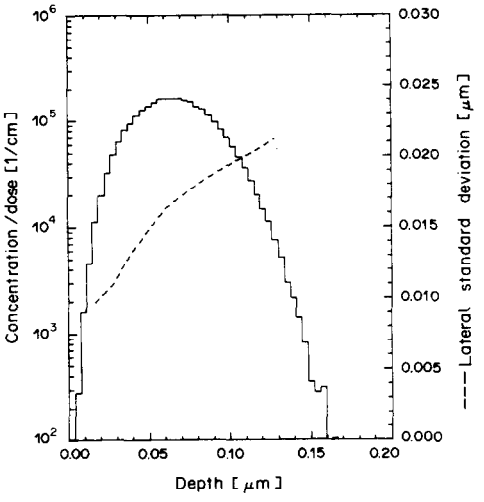

Fig. 1. Depth dependence of the lateral standard deviation for As in Si (100 keV).

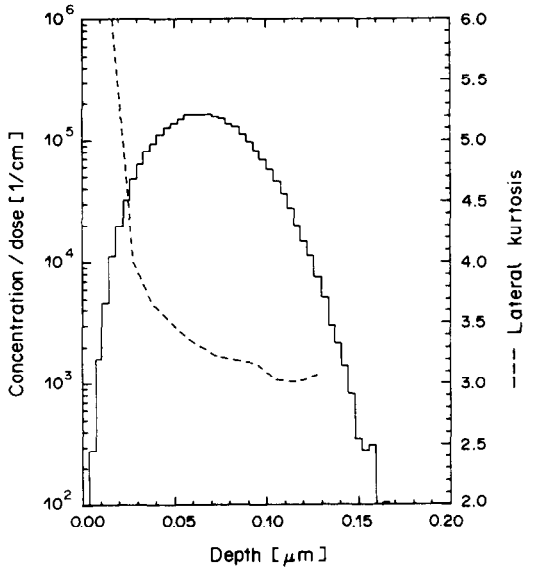

Fig. 2. Depth dependence of the lateral kurtosis for As in Si (100 keV).

for this is that the lateral standard deviation decreases towards the bulk (see Fig. 8; this is in contrast to the arsenic implantation of Fig. 1). Figures 5 and 6 show the results of our sophisticated analytical model and will be discussed in Section 4.3.

The statistical distribution function for one ion may generally be written:

$$f(z,x) = f_{\text{vert}}(z) f_{\text{lat}}(x,z). \tag{4}$$

$f_{\text{lat}}(x,z)$ is seen here as a function of x with parameters that depend on the lateral moments, which in turn are functions of the depth (z). In Section 4 we will specify $f_{\text{lat}}(x,z)$ as a function of lateral standard deviation σ_x and lateral kurtosis β_x. In Section 3 the functions $\sigma_x(z,E)$ and $\beta_x(z,E)$ will be given (E denoting the implantation energy) for the case of boron, phosphorus, arsenic, and antimony implantations into silicon in the range of 10–300 keV. These were obtained by fitting the results of our Monte-Carlo simulations. Also enclosed in Section 3 are fitting formulae for the vertical moments as a function of energy. Special features of our Monte-Carlo code are outlined in Section 2.

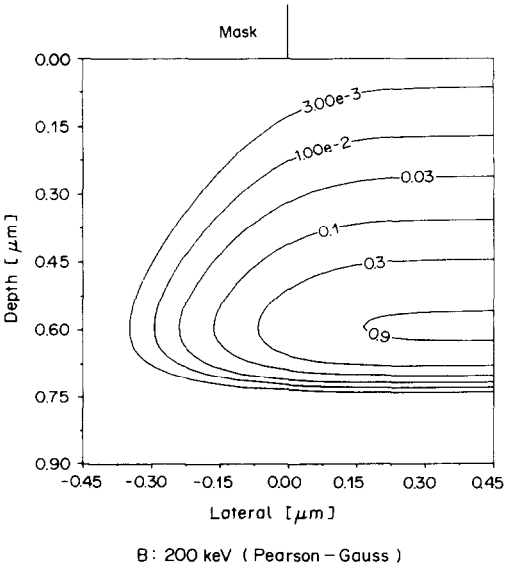

Fig. 3. Ion concentration below a vertical mask edge (B in Si, 200 keV): classical model, constant lateral standard deviation.

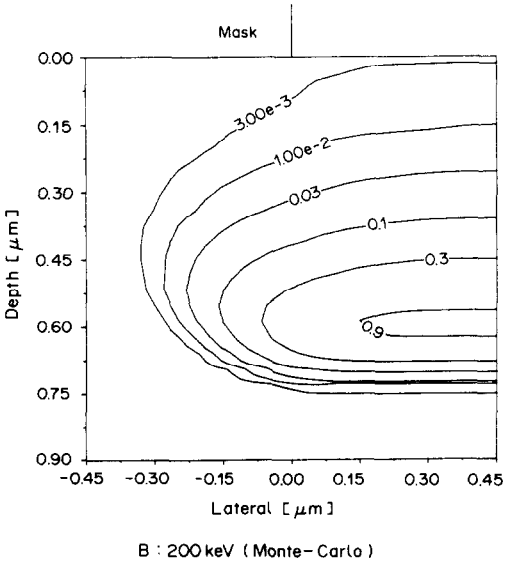

Fig. 4. Ion concentration below a vertical mask edge (B in Si, 200 keV): Monte-Carlo results.

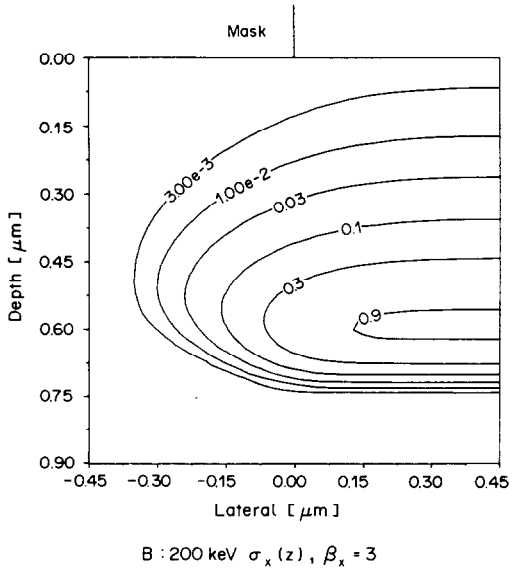

Fig. 5. Ion concentration below a vertical mask edge (B in Si, 200 keV): depth dependent lateral standard deviation, lateral kurtosis 3.

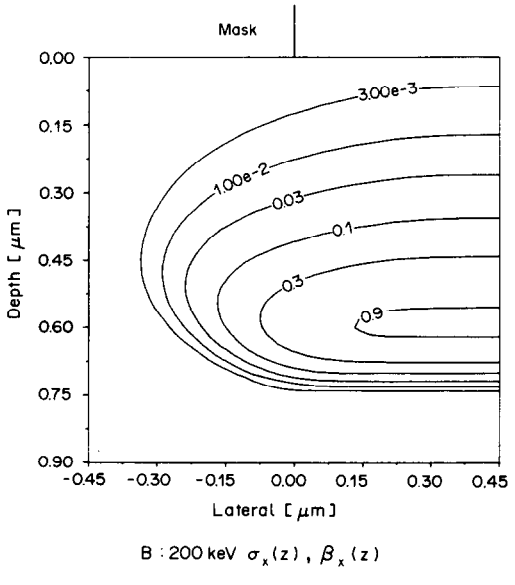

Fig. 6. Ion concentration below a vertical mask edge (B in Si, 200 keV): depth dependent lateral standard deviation and kurtosis.

2. DETAILS OF THE MONTE-CARLO SIMULATION

Among the Monte-Carlo codes for the simulation of ion implantation (e.g. Refs [18–20]) the "TRIM"-code of Biersack and Haggmark [20] has become most popular and has been used by a number of authors[21–23] because of its relative computer time efficiency. We have written our own code, based on the physical fundamentals of TRIM. In short, a large number of ion trajectories in an amorphous target are evaluated. Each ion undergoes collisions with target atoms (nuclei), which cause energy loss and deflection, and is additionally slowed down by interaction with target electrons. The Moliere potential is used to evaluate nuclear collisions and the Lindhard–Scharff formula to calculate electronic energy loss. Commonly, a correction factor of 1.5 to the Lindhard–Scharff formula is used for boron[10]. We, furthermore, employ a correction factor of 1.3 for phosphorus, which yields better agreement to some experimental profiles investigated by us. Recently the approach to the basic physics has been improved by Ziegler, Biersack and Littmark[24] (also reported in Ref. [9]), which has not yet been considered in our work.

Our code has some special features in order to increase computer time efficiency. First, the most time consuming part of conventional programs, the evaluation of nuclear collisions, is replaced by linear interpolation in two precomputed tables, which provide the scattering angle and the nuclear energy loss, respectively, as a function of impact parameter and energy. The strong nonlinearities in the dependence of the scattering quantities on impact parameter and energy and the limited dimension of the table (200×80) require the use of a nonlinear relation between table index and the corresponding values of the parameters. In this way we achieve an interpolation error of usually less than 10^{-3}. Only at very low energies (100 eV) deviations of some percent may occur.

Secondly, we use a special technique to calculate profiles with many different implantation energies simultaneously. For this purpose the ion starts with the greatest of these energies. When, during slowing down, the energy drops below the next implantation energy, its location and direction of motion are stored. From this, together with the final point of the trajectory, the coordinates of an ion which has been implanted with the lower implantation energy can be calculated. One complication, however, must be handled carefully: At a close collision with a nucleus the ion may lose a considerable part of its energy and thus fall far below the next implantation energy. If this happens, the ion obviously must not be taken into account. In the other case, when it falls only slightly below the next implantation energy, the final depth of the ion is corrected by an amount that corresponds to the increase of the mean projected range with implantation energy. The criterion when to omit an ion has been chosen pragmatically, so that at least 50% of the ions remain. In this procedure the deviation of the initial energies is always lower than 10% and, at the same time, lower than 10 keV. (For boron ions it is even less, namely 150 eV.) In several tests no difference could be detected between directly calculated profiles and those obtained with this procedure. So the criterion is rather too strong than too weak.

To make sure that we have not introduced un-

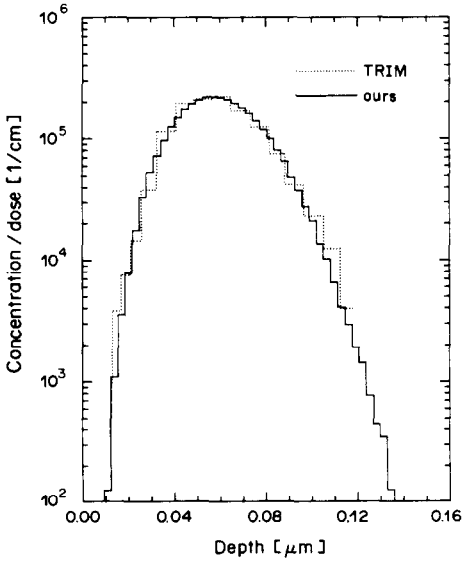

Fig. 7. Comparison of TRIM results (dotted line) with ours (full line) for Sb in Si (120 keV).

acceptable errors, we have also compared our results with that from TRIM. In Figure 7 a comparison of profiles for a 120 keV antimony implantation into silicon is shown. The dotted histogram has been taken from Ref. [24], the full line represents our results. No deviation can be seen which is clearly beyond statistical fluctuations.

Finally, we make use of the cylindrical symmetry of the statistical distribution function of an ion in order to reduce the noise of the lateral moments. For this purpose one could include the other lateral coordinate, i.e. one could replace the formula for the k-th lateral moment

$$m_k^{(x)} = \frac{1}{N} \sum_i x_i^k, \tag{5}$$

by

$$m_k^{(x)} = \frac{1}{2N} \sum_i (x_i^k + y_i^k). \tag{6}$$

This is permissible because x and y are distributed identically. Instead of this, we have employed a more elegant and in the context of our program simpler method: We first calculate the radial moment:

$$m_k^{(r)} = \frac{1}{N} \sum_i r_i^k, \tag{7}$$

$r_i = (x_i^2 + y_i^2)^{1/2}$, and then relate it to the lateral moment by:

$$m_k^{(x)} = \begin{cases} \frac{1}{2}\frac{3}{4}\cdots\frac{k-1}{k} m_k^{(r)} & \ldots k \text{ even} \\ 0 & \ldots k \text{ odd}. \end{cases} \tag{8}$$

This formula can be obtained by considering the definition of the moments via probability density functions and applying the rule of transforming probability density functions.

The evaluation of nuclear scattering can be replaced by look-up-tables in programs for crystalline target as well. The other two special features, however, are restricted to amorphous targets.

3. FITTING OF THE SPATIAL MOMENTS

We need the following spatial moments as input data for our analytical model:

—mean projected range $R_p(E)$
—vertical standard deviation $\sigma_z(E)$
—vertical skewness $\gamma_z(E)$
—vertical kurtosis $\beta_z(E)$
—lateral standard deviation $\sigma_x(z, E)$
—lateral kurtosis $\beta_x(z, E)$.

Tabulated values are available only for $R_p(E)$, $\sigma_z(E)$, $\gamma_z(E)$ and $\sigma_x(E)$[3, 4]. So we have calculated these quantities by means of Monte-Carlo method for 30 energies between 10 keV and 300 keV and in the case of lateral moments for approximately 40 intervals of depth. To obtain small statistical fluctuations the simulation has been performed with 100,000 (boron) to 200,000 (antimony) ions. The results were then fitted by the below specified formulae.

3.1. Vertical moments

If the reader wants to get an idea of the qualitative dependence of the four moments on the implantation energy, see Ref.[21], where a graphic representation of the moments is given for the four elements. (The results of Ref.[21] are close to ours). We have chosen the following fitting formulae for the vertical moments:

$$\mathrm{R_p(E)} = a_1 E^{a_2} + a_3 \tag{9a}$$

$$\sigma_z(E) = a_1 E^{a_2} + a_3 \tag{9b}$$

$$\gamma_z(E) = \frac{a_1}{a_2 + E} + a_3 \tag{9c}$$

$$\beta_z(\mathrm{E}) = \frac{a_1}{a_2 + E} + a_3 + a_4 E. \tag{9d}$$

The units used for the implantation energy E are keV, for all lengths (R_p, σ_z) μm are used. The parameters are listed in Tables 1–4.

Note the fitting formulae are valid only in the range of 10–300 keV. We have tried to produce formulae that behave reasonably outside this range.

Table 1. Projected range R_p

	Boron	Phosphorus	Arsenic	Antimony
a_1	0.00969	0.001555	0.000688	0.000668
a_2	0.767	0.958	0.983	0.921
a_3	−0.01815	0.000828	0.003962	0.005072
MSE	1.41%	0.57%	0.59%	0.57%

MSE denotes the mean square error.

Table 2. Vertical standard deviation σ_z

	Boron	Phosphorus	Arsenic	Antimony
a_1	0.0521	0.002242	0.000402	0.000241
a_2	0.216	0.659	0.874	0.884
a_3	−0.0684	−0.003435	0.000582	0.000923
MSE	1.92%	1.73%	0.30%	0.35%

MSE denotes the mean square error.

Table 3. Vertical skewness γ_z

	Boron	Phosphorus	Arsenic	Antimony
a_1	312.7	336.2	339.8	195.1
a_2	122.2	199.3	342.0	339.7
a_3	−2.404	−1.386	−0.5051	−0.0910
MSE	0.0235	0.0093	0.0047	0.0068

MSE denotes the mean square error.

Table 4. Vertical kurtosis β_z

	Boron	Phosphorus	Arsenic	Antimony
a_1	0.0	54.45	38.73	47.33
a_2	1.0	55.74	61.70	81.17
a_3	2.212	1.865	2.559	2.692
a_4	0.0195	0.00482	0.0	0.0
MSE	1.66%	0.39%	0.60%	0.58%

MSE denotes the mean square error.

Nevertheless R_p and σ_z do not approach 0 for implantation energy 0. Avoiding this would have resulted either in a considerable increase of the fitting error or in a more complex formula. So, if one insists on using our data for implantation energies less than 10 keV, one should interpolate R_p and σ_z linearly between 0–10 keV.

3.2. *Lateral moments*

The results for the lateral standard deviation are shown in Figs 8–11. Note that the representation in Figs 8 and 9 must be rotated by 90° to be compared with Figs 10 and 11. The lateral standard deviation of heavy ions (As, Sb) increases towards the bulk, quite opposite to the case of light ions (B). The physical reason might be this: Heavy ions can be scattered in a single collision with a target atom only by small angles. (E.g. the maximum deflection angle of an As atom in a collision with a Si atom is 20°). So heavy ions are very unlikely to change direction and to come back towards the surface if they have already penetrated into deeper regions. On the other hand, they may stop after a few close collisions without having moved in the lateral direction. So the lateral standard deviation near the surface is small, whereas it increases towards the bulk because of the spreading of the beam.

In contrast, light ions may be deflected by angles up to 180°, and they may be scattered into the lateral direction without losing most of their energy. This accounts for the great standard deviation. Moreover, the slowing down is dominated by the electronic energy loss, which gives rise to an upper limit of the total path length. For this reason, unless an ion is travelling nearly perpendicular to the surface, it is not able to reach the maximum profile depth. So the lateral standard deviation will decrease towards the bulk, if the electronic stopping power dominates.

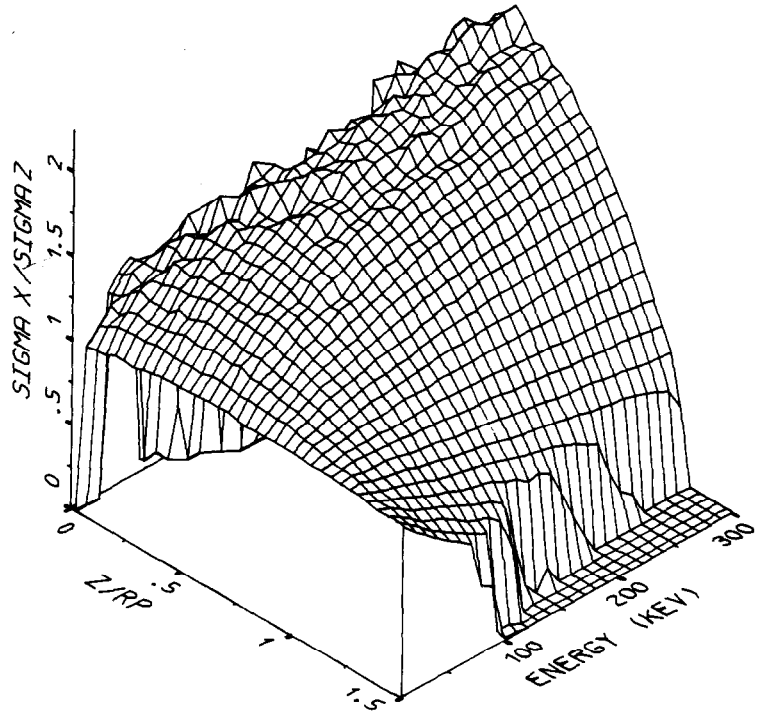

Fig. 8. $\sigma_x(z, E)$ for B in Si.

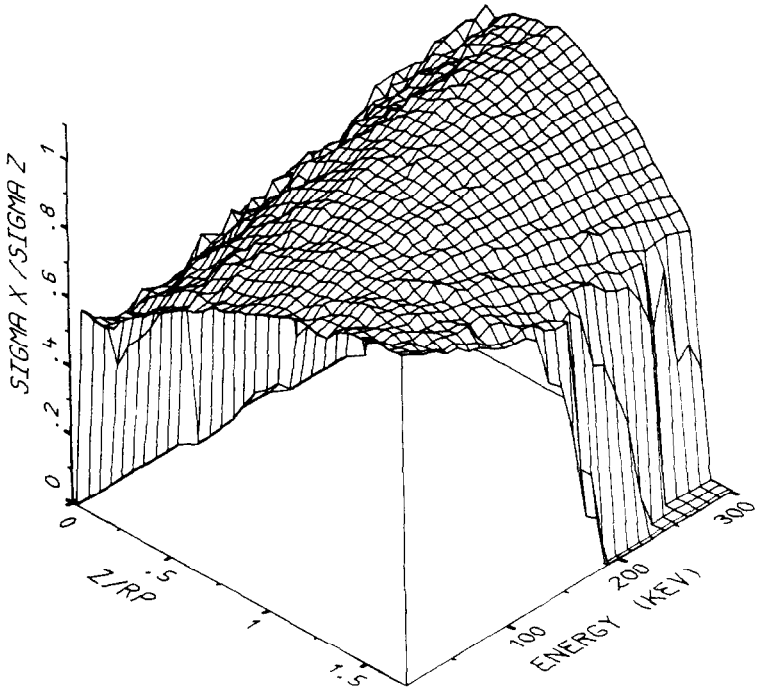

Fig. 9. $\sigma_x(z, E)$ for P in Si.

From Figures 8–11 one can also see why Giles and Gibbons[23] come to the conclusion that—in opposition to the message of our paper—the correlation between the vertical and lateral coordinate may be neglected; They have unfortunately proven their theory with a 20 keV boron implantation, which is more or less the only example of a nearly constant lateral standard deviation.

Figures 12 and 13 show the lateral kurtosis for boron and phosphorus. The figures for arsenic and antimony are similar to that of phosphorus. It is noticed that the kurtosis is always less than 3 for

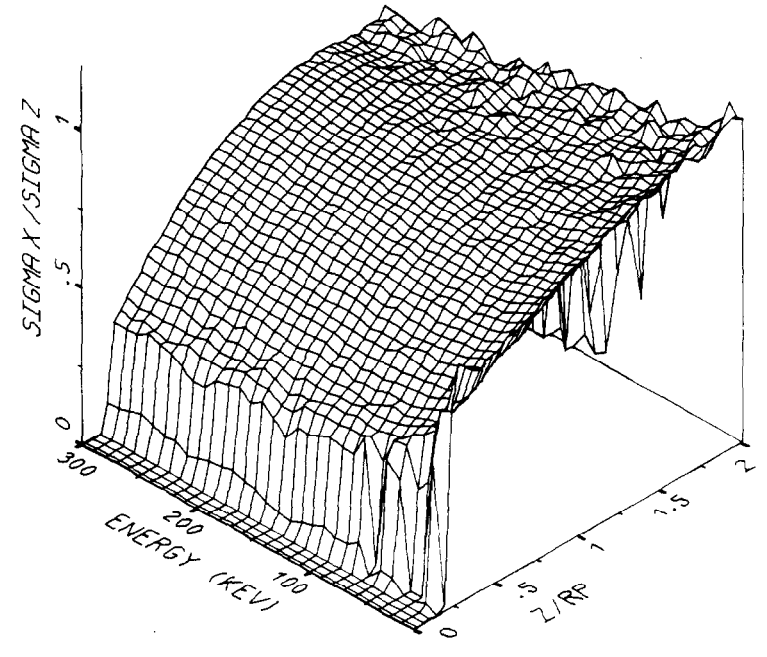

Fig. 10. $\sigma_x(z, E)$ for As in Si.

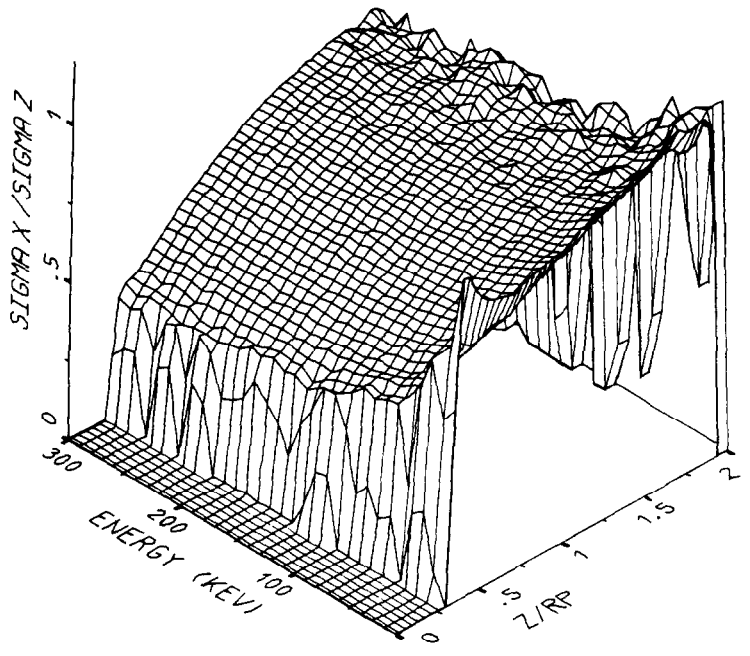

Fig. 11. $\sigma_x(z, E)$ for Sb in Si.

boron and that for the heavy elements large kurtoses are possible near the surface.

Fitting 2-D tables requires more complex formulae. We use:

$$\sigma_x(z, E) = \sigma_z(E)\left\{\frac{1}{a_1}\ln[\exp(a_1 P_1) + \exp(a_1 P_2)]\right\}, \tag{10a}$$

$$\beta_x(z, E) = \frac{1}{a_1}\ln[\exp(a_1 P_1) + \exp(a_1 P_2)], \tag{10b}$$

with

$$P_1 = a_2 z' E + a_3 z' + a_4 E + a_5, \tag{11a}$$

$$P_2 = a_6 z' E + a_7 z' + a_8 E + a_9, \tag{11b}$$

and z' the reduced depth:

$$z' = z/R_p(E). \tag{11c}$$

The parameters a_1–a_9 are listed in Tables 5 and 6.

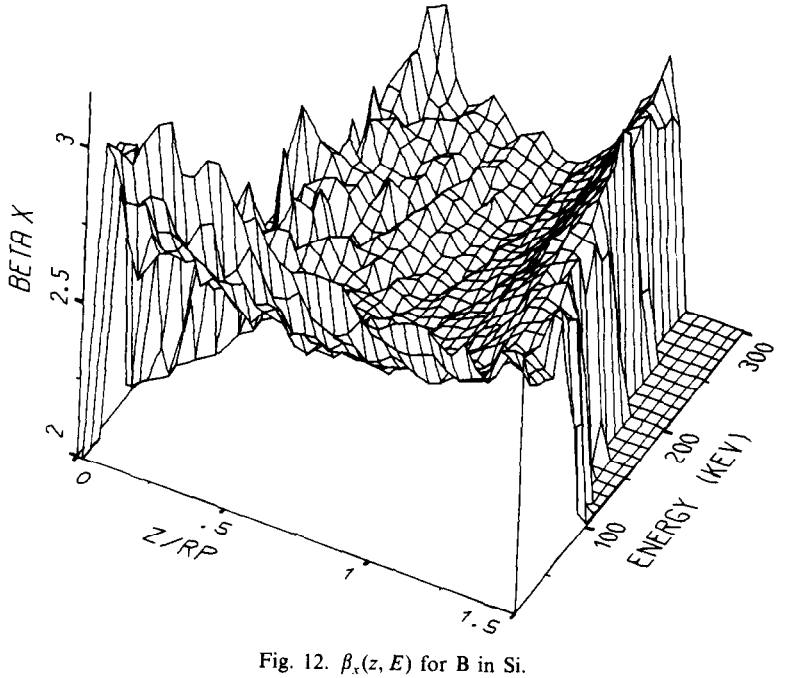

Fig. 12. $\beta_x(z, E)$ for B in Si.

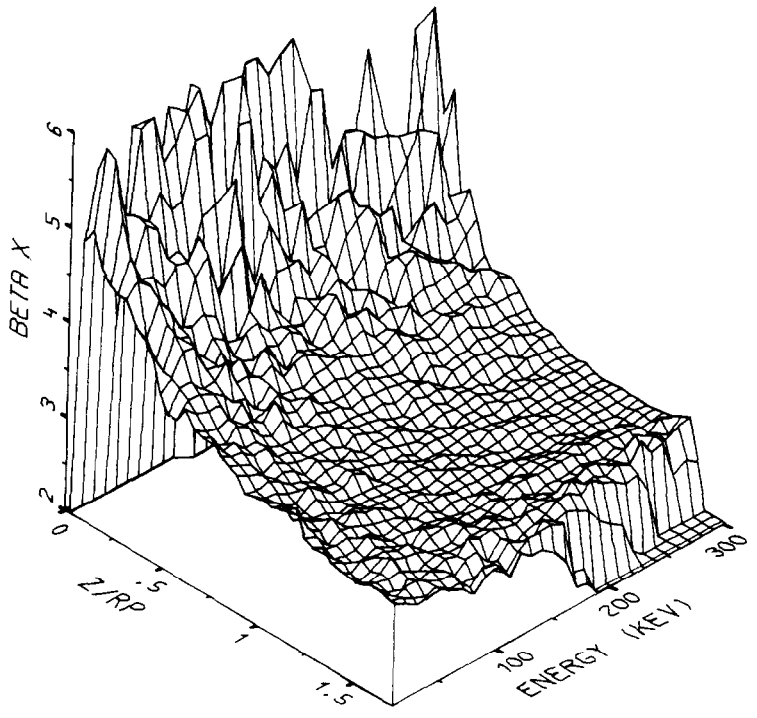

Fig. 13. $\beta_x(z, E)$ for P in Si.

It is not reasonable to give a fitting error here, because one could hardly decide if the error is due to fluctuations of the Monte-Carlo results or to bad approximation. Instead, we have plotted the fitted and the unfitted moments in a 3-D representation. An example is shown in Fig. 14, which may be compared with Fig. 8.

4. ANALYTICAL MODEL

4.1. Vertical distribution function

We do not intend to present a new vertical distribution function here, but we want to point out a problem with the Pearson IV distribution, which arises together with moments derived from Monte-Carlo calculations (it has already been encountered by Peterson *et al.*[21]): Skewness and kurtosis violate an inequality that restricts the applicability of the Pearson IV distribution. On the other hand, the Pearson IV function fits experimental profiles well in many cases[5–9]. The reason for this discrepancy is that real implantations are performed into crystalline targets where always a certain amount of channeling occurs.

There are various possibilities to overcome this problem. First, one can simply modify the moments to meet the inequality between skewness and kurtosis. If one maintains the skewness, one has to increase the kurtosis by 10–20% which seems to be acceptable. (This has been done in Figs 3–6). Another way is to perform a 1-D Monte-Carlo simulation to obtain the vertical distribution function directly. This is in many cases feasible, because computer time efficiency of Monte-Carlo programs has increased considerably. The last possibility is to use an experimental profile for the vertical distribution. However, this method should be handled carefully, because if there is too much channeling in the profile, our data for the lateral standard deviation could possibly not apply.

Table 5. Lateral standard deviation σ_x

	Boron	Phosphorus	Arsenic	Antimony
a_1	−1.443	−0.9488	−6.724	−13.884
a_2	−0.005637	0.002793	0.000582	0.000481
a_3	1.558	1.205	0.5117	0.3685
a_4	0.003511	−0.001370	−0.000649	−0.001024
a_5	1.189	1.043	0.3709	0.4838
a_6	−0.013185	−0.003208	−0.000512	−0.000110
a_7	−0.2271	−0.1201	0.1299	0.1357
a_8	0.014883	0.003528	0.000375	−0.000425
a_9	1.422	1.320	0.7277	0.7529

Table 6. Lateral kurtosis β_x

	Boron	Phosphorus	Arsenic	Antimony
a_1	0.5278	0.03496	1.134	6.462
a_2	0.002498	−0.2996	−0.01340	−0.005668
a_3	−0.9765	−60.76	−2.927	−0.4474
a_4	−0.000061	0.008940	0.007873	0.004384
a_5	2.538	−53.66	4.493	3.345
a_6	0.02713	−0.001406	−0.000965	−0.000613
a_7	0.5976	0.2740	−0.06646	−0.11157
a_8	−0.03790	0.001470	0.001077	0.000901
a_9	0.5911	2.504	3.224	3.246

4.2. Lateral distribution function

We look for a function $f(x)$ with the following characteristics: symmetry; positivity; only one max-

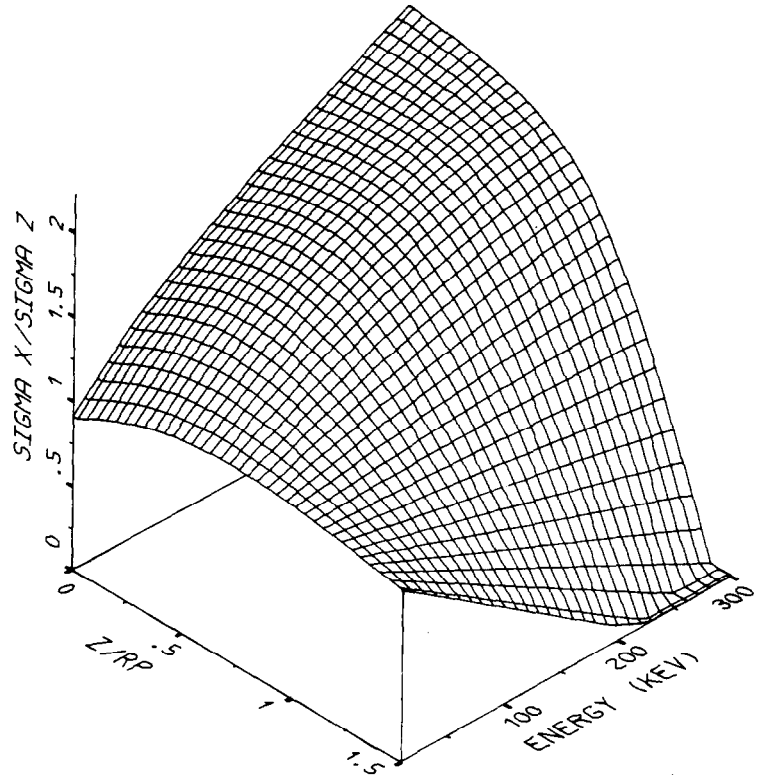

Fig. 14. $\sigma_x(z, E)$ for B in Si (fitted).

imum; smoothness; its parameters can be calculated from standard deviation σ and kurtosis β. For that purpose the moments must exist to the fourth order.

A. Modified Gaussian distribution—The function $f(x)$ has to meet the equations:

$$1 = \int_{-\infty}^{\infty} f(x)\,\mathrm{d}x, \tag{12a}$$

$$\sigma^2 = \int_{-\infty}^{\infty} x^2 f(x)\,\mathrm{d}x, \tag{12b}$$

$$\beta\sigma^4 = \int_{-\infty}^{\infty} x^4 f(x)\,\mathrm{d}x. \tag{12c}$$

Thus we need (at least) 3 free parameters. The Gaussian function:

$$f(x) = a\exp(-(bx)^2) \tag{13}$$

has only two parameters, which are determined by equation (12a) and equation (12b):

$$a = \frac{1}{\sqrt{2\pi}\,\sigma}, \tag{14a}$$

$$b = \frac{1}{\sqrt{2}\,\sigma}. \tag{14b}$$

The kurtosis equals 3 in any case. In order to obtain one additional parameter, we replace the power 2 in the Gaussian function equation (13) by an arbitrary power p:

$$f(x) = a\exp(-|bx|^p). \tag{15}$$

Introducing equation (15) into (12), we need the integral [25]:

$$\int_0^{\infty} x^n \exp(-|bx|^p)\,\mathrm{d}x = \Gamma\left(\frac{n+1}{p}\right)\Big/(p\,b^{n+1}). \tag{16}$$

Γ denotes the Gamma function. β can be expressed, using equation (12):

$$\beta = \frac{\Gamma(1/p)\,\Gamma(5/p)}{\Gamma(3/p)^2}. \tag{17}$$

We need the inverse function of equation (17), what unfortunately cannot be done analytically. So we have solved the problem for very large p:

$$\left(\frac{1}{p}\right)_0 = 0.290576\sqrt{\beta - 1.8} \tag{18a}$$

and for very small p:

$$\left(\frac{1}{p}\right)_\infty = 0.687042\ln\left(\frac{\sqrt{5}\,\beta}{3}\right). \tag{18b}$$

The actual value of $1/p$ is obtained by interpolation

$$\frac{1}{p} = c\left(\frac{1}{p}\right)_0 + (1-c)\left(\frac{1}{p}\right)_\infty, \tag{18c}$$

with

$$c = 0.795833 \exp[-1.94544(\beta - 1.8)] + 0.204167 \exp[-0.272172(\beta - 1.8)]. \quad (18d)$$

Equation (18d) was fitted to 100 (β, p)-values in the range $1.8 < \beta < 6$. The mean square error is about 1%, but it is centered at very small β, so the error in the relevant range of β is less (e.g. $\beta = 3$ leads to $p = 1.999$ instead of 2, which is correlated by equation (17) to $\beta = 3.001$).

With p from equation (18c) one obtains easily

$$b = \frac{1}{\sigma}\sqrt{\Gamma\left(\frac{3}{p}\right)\Big/\Gamma\left(\frac{1}{p}\right)} \quad (19)$$

and

$$a = (b\,p)\Big/\left(2\,\Gamma\left(\frac{1}{p}\right)\right). \quad (20)$$

Equation 15 is shown in Fig. 15 for various values of β. For $\beta = 6$ $(p = 1)$ the derivation of $f(x)$ at $x = 0$ is discontinuous and for $\beta > 6$ it becomes infinite. In the case of ion implantation profiles, lateral kurtoses >6 do practically not appear. However, from a general point of view it might be interesting to give a function that may be used for arbitrary large kurtoses. (Extremely high lateral kurtoses appear e.g. with damage profiles.)

B. Pearson VII Distribution—A function that can be applied for $\beta > 3$ is the Pearson VII distribution [26]:

$$f(x) = C\left|1 + \frac{b_2}{b_0}x^2\right|^{1/2b_2}, \quad (21)$$

b_0 and b_2 are given by:

$$b_0 = -\frac{2\beta\sigma^2}{5\beta - 9} \quad (22a)$$

$$b_2 = -\frac{\beta - 3}{5\beta - 9}. \quad (22b)$$

To evaluate the constant C we need [27]:

$$\int_{-\infty}^{\infty}(1 + x^2)^p\,dx = B(\tfrac{1}{2}, -p - \tfrac{1}{2}). \quad (23)$$

B denotes the Beta function, which is defined by the Gamma function by:

$$B(x, y) = \frac{\Gamma(x)\,\Gamma(y)}{\Gamma(x + y)}. \quad (24)$$

One obtains:

$$C = \sqrt{\frac{b_2}{\pi\,b_0}}\,\frac{\Gamma(-1/2b_2)}{\Gamma(-1/2b_2 - 1/2)}. \quad (25)$$

The Pearson VII function is shown in Fig. 16 for some values of β. It tends asymptotically towards the Gaussian function, if β tends towards 3. So it is well suited to be used for $\beta > 3$ together with the modified Gaussian distribution for $\beta < 3$.

4.3. Distribution under a mask edge

Considering σ and β as functions of z $[\sigma_x(z, E), \beta_x(z, E)]$, $f(x)$ of the previous section may be called $f_{\text{lat}}(x, z)$. Multiplication with the vertical distribution function $f_{\text{vert}}(z)$ yields the 2-D distribution function for one ion [cf. equation (4)]. This distribution function can then be used in a convolution integral to calculate the distribution function under a mask edge[11, 12, 16, 9]. We do not discuss the convolution integral here, but we note that it does not treat those ions correctly which leave the mask into the air and re-enter the target.

The results of our calculations for an infinitely steep mask edge are shown in Figs 5 and 6. In both cases the vertical distribution function has been assumed a Pearson IV function. The vertical kurtosis has been modified as mentioned in Section 4.1, what accounts for the slight difference in the vertical profile, which can be seen at the right hand side of the simulation area. In Figure 5 the lateral kurtosis has been assumed $\beta = 3$, so we have a Gaussian distribu-

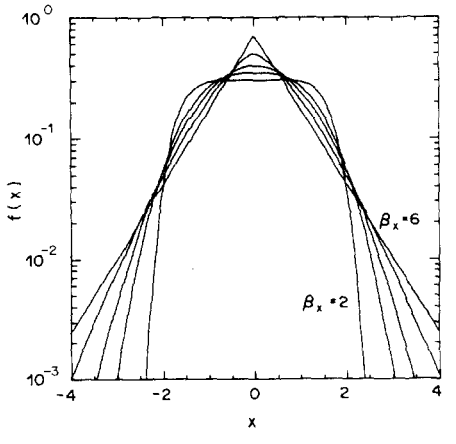

Fig. 15. Modified Gaussian distribution for $\sigma_x = 1$ and $\beta_x = 2, 2.5, 3, 4, 6$.

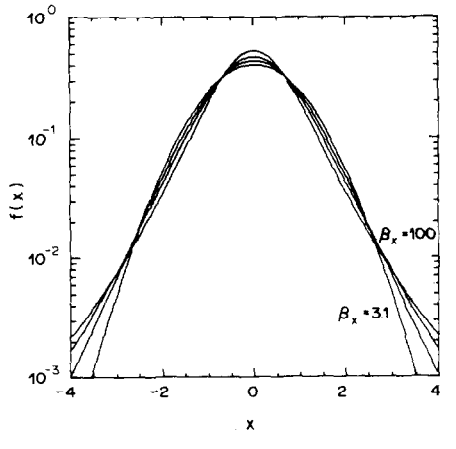

Fig. 16. Pearson VII distribution for $\sigma_x = 1$ and $\beta_x = 3.1, 4, 6, 100$.

tion laterally, but with a depth dependent standard deviation. In Figure 6 we also take into account the lateral kurtosis.

Figures 5 and 6 seem to indicate that the correct lateral kurtosis yields no significant improvement. So allowing for the lateral kurtosis might be oversophisticated, especially if one considers that our data may deviate from real implantations in crystalline silicon for light ions. On the other hand, larger errors due to neglecting lateral kurtosis appear for heavy ions in regions close to the surface, where no channeling occurs.

5. CONCLUSION

A two-dimensional model of ion implantation has been presented, which allows for depth dependent lateral standard deviation and kurtosis. The moments were given in Section 3 by simple formulae. Distribution functions which allow to include the lateral kurtosis were presented in Section 4. How to use them to calculate the distribution below a mask edge, is found in the cited literature.

A comparison with experimental data could not be done, because 2-D profile measurements are not possible at present. It can be expected that our data apply well for heavy ions, where no channeling occurs, but deviations are likely for the light ion species boron. In order to investigate this, it would be interesting to perform a Monte-Carlo simulation with a program for crystalline targets.

Acknowledgements—This work was supported by the research laboratories of SIEMENS AG at Munich, FRG and by the "Fonds zur Foerderung der wissenschaftlichen Forschung", project S43/10. We are very grateful to Professor H. Poetzl for carefully reading the manuscript.

REFERENCES

1. J. Lindhard, M. Scharff and H. E. Schiøtt, *Mat.-fys. Meddr* **33,** 14 (1963).
2. J. F. Gibbons and S. Mylroie, *Appl. Phys. Lett.* **22,** 568 (1973).
3. H. Ryssel and I. Ruge, *Ionenimplantation* Teubner, Stuttgart (1978).
4. J. F. Gibbons, W. S. Johnson and S. W. Mylroie, *Projected Range Statistics* Halstead Press, Stroudsburg (1975).
5. H. Ryssel, K. Haberger, K. Hoffmann, G. Prinke, R. Duemcke and A. Sachs, *IEEE Trans. Electron Dev.* **ED-27,** 1484 (1980).
6. F. Jahnel, H. Ryssel, G. Prinke, K. Hoffmann, K. Mueller, J. Biersack and R. Henkelmann, *Nucl. Instrum. Meth.* **182/183,** 223 (1981).
7. H. Ryssel, G. Prinke, K. Haberger, K. Hoffmann, K. Mueller and R. Henkelmann, *Appl. Phys.* **24,** 39 (1981).
8. M. Simard-Normandin and C. Slaby, *J. Electrochem. Soc.* **132,** 2218 (1985).
9. H. Ryssel and J. P. Biersack, *Process and Device Modeling*, (Edited by W. L. Engl), pp. 31–69. Elsevier, North Holland (1986).
10. W. K. Hofker, D. P. Oosthoek, N. J. Koeman and H. A. M. De Grefte, *Radiat. Eff.* **24,** 223 (1975).
11. S. Furukawa, H. Matsumura and H. Ishiwara, *Jap. J. appl. Phys.* **11,** 134 (1972).
12. H. Runge, *Physica Status Solidi.* **39a,** 595 (1977).
13. D. A. Antoniadis, S. E. Hansen and R. W. Dutton, Report 5019-2, Stanford University (1978).
14. R. Tielert, *IEEE Trans. Electron Dev.* **ED-27,** 1479 (1980).
15. K. Taniguchi, M. Kashiwagi and H. Iwai, *IEEE Trans. Electron Dev.* **ED-28,** 574 (1981).
16. S. Selberherr, *Analysis and Simulation of Semiconductor Devices* Springer, New York (1984).
17. H. Ryssel, Proc. VLSI Process and Device Modeling, Katholieke Universiteit Leuven (1983).
18. A. Desalvo, R. Rosa and F. Zignani, *J. appl. Phys.* **43,** 3755 (1972).
19. M. T. Robinson and I. M. Torrens, *Phys. Rev.* **9B,** 5008 (1974).
20. J. P. Biersack and L. G. Haggmark, *Nucl. Instrum. Meth.* **174,** 257 (1980).
21. W. P. Petersen, W. Fichtner and E. H. Grosse, *IEEE Trans. Electron Dev.* **ED-30,** 1011 (1983).
22. J. Albers, *IEEE Trans. Comp.-Aided Des.* **CAD-4,** 374 (1985).
23. M. D. Giles and J. F. Gibbons, *J. Electrochem. Soc.* **132,** 2476 (1985).
24. J. F. Ziegler, J. P. Biersack and U. Littmark, *The Stopping and Range of Ions in Solids* Pergamon Press, New York (1985).
25. I. S. Gradshteyn and I. M. Ryzhik, *Table of Integrals, Series and Products. Corrected and Enlarged Edition*, p. 342. Academic, New York (1980).
26. N. L. Johnson and S. Kotz, *Continuous Univariate Distributions*-1 Houghton Mifflin Company, Boston (1970).
27. I. S. Gradshteyn and I. M. Ryzhik, *Table of Integrals, Series and Products. Corrected and Enlarged Edition*, p. 295. Academic, New York (1980).